On the effects of uncertain amounts of residual impurities in shock-tube measurements of hydrogen ignition times

By J. Urzay, N. Kseib, D. F. Davidson†, G. Iaccarino AND R. K. Hanson†

1. Motivation and objective

This study addresses the influences of uncertain amounts of residual impurities in the computation and experimental determination of ignition-delay times in hydrogen-air mixtures in shock tubes. Experimental methods for quantifying impurities in shock tubes are described and utilized. These methods are utilized to infer an equivalent amount of impurities as a function of the initial temperature of the mixture in the shock tube. A statistical model of the concentration of impurities is constructed and used for calculations of ignition delays based on short and detailed chemical descriptions.

2. Background

The parameters of practical chemical systems are rarely sufficiently well quantified to warrant less than 10% uncertainty in ignition delays obtained from calculations or experiments. Many of these uncertain parameters are related to chemical-kinetic rate constants, which abound in fuels that involve hundreds of reactions. Other uncertainties may be related to transport effects, in that flow strain, temperature inhomogeneities and composition gradients could develop in the mixture under some conditions, which may be needed to be accounted for if accurate predictions of ignition phenomena are pursued.

Additional sources of uncertainties in explosive systems can be related to the initial thermodynamic conditions and chemical composition of the mixture. This last type uncertainty represents an important issue in ambients where the reactive mixture cannot be monitored directly with precision. Paradoxical examples of situations where the mixture conditions are extremely difficult to characterize can be found in explosions in water-cooled nuclear reactors (USNRC 1979; NISA Japan 2011). In nuclear reactors, gaseous hydrogen (H_2) is produced in increasingly large quantities under high temperatures from the oxidation of the Zirconium alloy that covers the fuel rods. Hydrogen can leak accidentally from the primary circuit or be intentionally vented to relieve pressure in nuclear emergencies, which leads to dangerous combustible bubbles in the containment dome and, eventually, to uncontrolled autoignition and explosions. Deterministic measures of mixture ignitability may therefore not be the best option in these situations.

To the same family of problems that involve ignition of uncertain mixtures belongs the uncontrolled contamination of shock tubes with residual impurities. Shock tubes are often used to measure ignition times (Davidson & Hanson 2004). Despite being much more accurate than other measuring devices, shock tubes are subject to a number of imperfections. Figure 1 depicts some of these limitations in the case of $H_2 - O_2$ ignition.

† High Temperature Gasdynamics Laboratory, Mechanical Engineering Department, Stanford University.

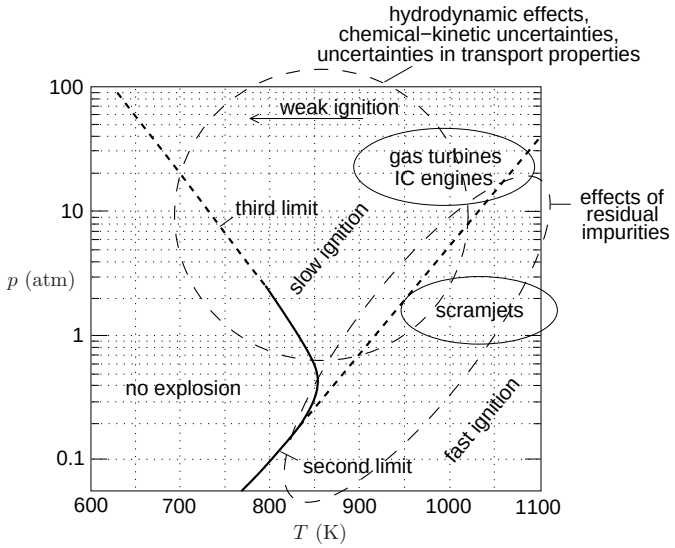

FIGURE 1. Explosion diagram for stoichiometric H_2/O_2 mixtures (adapted from Lewis & von Elbe (1961)). The diagram includes typical operating conditions in propulsion systems, as well as some of the dominant effects that induce uncertainties in shock-tube measurements and computations of H_2/O_2 ignition.

For temperatures well above the second explosion limit and its prolongation, the ignition times are fast compared to any transport phenomena in the shock tube, and ignition occurs in a mostly homogeneous environment. In these conditions, the shock tube provides accurate values of ignition delays. The accuracy of analytical calculations of ignition delays in this regime is limited only by the small uncertainties in the rates of the dominant chemical steps, among which the rate of $H + O_2 \rightarrow OH + O$ is the most important. As conditions approach the crossover temperature from above, the effects of the residual impurities in the shock tube are dominant and induce uncertainties of order 10-20% in ignition delays of undiluted mixtures, with these effects becoming more important (up to 40%) in highly diluted mixtures (Urzay *et al.* 2014). Below crossover, and towards the third-explosion limit, the effects of the impurities are negligible, but the ignition time is sufficiently long for transport effects to become important in the shock tube. In this regime, boundary layer detachment, the presence of isolated ignition kernels, and flame propagation occur in the shock tube, with conditions rapidly departing from the idealized homogeneous-reactor limit (Ihme *et al.* 2013). In addition, in computations of the ignition time near the third explosion limit, the uncertainties in chemical steps involving hydrogen peroxide (H_2O_2) become important, and among them, the uncertainties in the rate of $HO_2 + H_2 \rightarrow H_2O_2 + H$ lead to 50% variations in the pressure of the third explosion limit (Sánchez *et al.* 2014).

In this report, focus is directed to the effects of residual impurities. The remainder of this report is organized as follows. In Section 3, experimental methods are used to quantify impurities in shock tubes, and a statistical model of the impurities concentration is described. In Section 4, the effects of the impurities on ignition delays above crossover are analyzed using short and detailed chemical descriptions. Section 5 is focused on conditions near and below crossover. Lastly, conclusions are drawn in Section 6. Additional

results and considerations, including the treatment of diluted mixtures and the effects of chemical-kinetic uncertainties, are given in Urzay *et al.* (2014).

3. Experimental quantification of impurities in shock tubes

In shock tubes, residual radicals may be generated by the decomposition of long-chained hydrocarbon molecules. These large molecules may be present in the shock tube because of three main reasons: i) they remain in the tube as leftovers of previous experiments, ii) they are introduced by cleaning substances for shock-tube maintenance, iii) they are products generated by decomposition of the organic compounds which gaskets, seals, diaphragms, and wall coatings are made of. Among all sources of impurities, non-volatile compounds at room temperature, in particular heavy hydrocarbons, are most likely to be adsorbed onto surfaces and remain in the tube. To worsen the problem, these contaminants remain in the shock tube even after gas-exchange processes, ultra-vacuum pumping, and meticulous cleaning procedures. These compounds act as radical precursors. As the test gas mixture is blown into the shock tube, it comes in contact with the supply tubing and with the shock tube wall. Exchange with surface contaminants and with outgassing from crevices in the shock tube puts the radical precursors into the bulk gas. The diaphragm rupture and laser measurements typically occur within 1 minute after filling. When the shock wave passes through the bulk gas, the high temperatures decompose the radical precursors and form radicals such as H-atoms. Despite being supported by common experience, the above explanation is only qualitative and more research is needed in order to assess the exact causes of formation of impurities in shock tubes.

The exact composition of the impurities pool is also extremely difficult and often impractical to characterize in shock-tube normal operating conditions. However, an equivalent amount of H impurities can be inferred by using any of the following two methods proposed here: $\mathcal{M}_1$) "a-priori OH absorption in unfueled mixtures", and $\mathcal{M}_2$) "a-posteriori comparison of fueled experimental data with calculations". These methods are described in Urzay *et al.* (2014). Experimental data obtained using these methods are shown in Figure 2, in which an equivalent amount of H impurities is obtained for a range of operating temperatures in a number of shock tubes in the Shock-Tube Facilities of the High-Temperature Gasdynamics Laboratory at Stanford. Given the standardized cleaning procedures used for the operation of these facilities, the experimental results shown in Figure 2 are most likely representative of the temperature distribution of impurities in any other typical shock tube. As depicted in Figure 2, the concentration of radical impurities tends to increase for increasing temperatures because of the increasingly faster activation of the radical precursors.

In a hierarchy of possible models, the results in Figure 2 suggest a simple Arrhenius model

$$X_{\mathrm{H},0} = \xi \overline{X}_{\mathrm{H},0}, \quad \text{with} \quad \overline{X}_{\mathrm{H},0} = A_{\mathrm{H}} \mathrm{e}^{-T_{a,\mathrm{H}}/T} \quad (\mathrm{ppm}), \tag{3.1}$$

for the molar fraction of H-impurities $X_{\mathrm{H},0}$, where $T_{a,\mathrm{H}} = 12916$ K is the activation temperature and $A_{\mathrm{H}} = 682.93$ ppm is a pre-exponential factor. In this formulation, ξ is a dimensionless log-normal random variable given by

$$\ln \xi \sim \mathcal{N}(0, \sigma_{\mathrm{H}}^2), \quad \text{with} \quad \sigma_{\mathrm{H}}^2 = \frac{1}{4} \ln^2 \mathrm{UF}_{\mathrm{H}}, \tag{3.2}$$

where σ is the standard deviation, and UF_{H} is an uncertainty factor described below. In

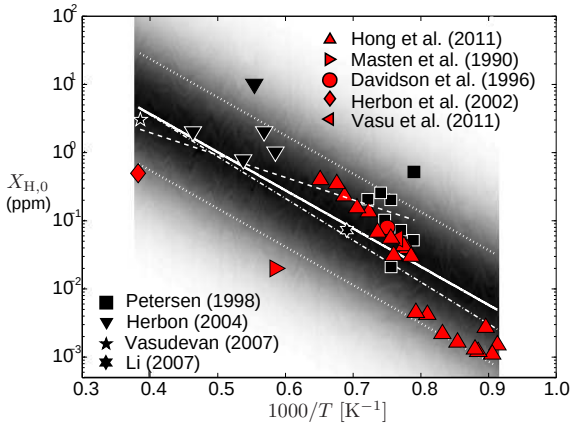

FIGURE 2. Equivalent concentration of H impurities measured in the Stanford Shock-Tube Facilities as a function of the inverse of the temperature. The shaded contours indicate the PDF of H-impurities concentration $P(X_{\mathrm{H},0})$ given by the stochastic model of impurities in Eq. (3.1)-(3.2), with dark and white regions indicating high and low probability, respectively. The dotted lines represent one standard deviation from the linear regression curve (solid line) as given by Eq. (3.2). Dot-dashed and dashed lines represent linear regression models if data obtained by using either $\mathcal{M}_1$ or $\mathcal{M}_2$ are retained, respectively.

this analysis, the temperature T is assumed to be a known parameter in the calculations. The effects of the temperature uncertainties on delay times obtained from shock-tube experiments are briefly explored in Section 5.

Equation (3.1) represents a thermal-activation process for the generation of impurities, in which the nominal Arrhenius parameters A_{H} and $T_{a,\mathrm{H}}$ are obtained by a least-squares approximation. Equations (3.1) and (3.2) imply the use of a Gaussian distribution for the PDF $P(\ln X_{\mathrm{H},0})$, which is a model that proves to be accurate to describe the multiplicative spread of data observed at increasing temperatures. Therefore, $\ln \overline{X}_{\mathrm{H},0}$ represents the mean, mode, and expectation of $\ln X_{\mathrm{H},0}$. Similarly, $\overline{X}_{\mathrm{H},0}$ and $\overline{X}_{\mathrm{H},0}\exp(-\sigma_{\mathrm{H}}^2)$ are the median and mode of $X_{\mathrm{H},0}$, respectively. The expectation of the impurities distribution is $\mathrm{E}[X_{\mathrm{H},0}] = \overline{X}_{\mathrm{H},0}\exp(\sigma_{\mathrm{H}}^2/2)$, which should not be confused with $\overline{X}_{\mathrm{H},0}$.

In Equation (3.2), a notation based on the uncertainty factor UF_{H} has been used, which is widely employed in the assessment of chemical-kinetic uncertainties. In particular, $\ln \mathrm{UF}_{\mathrm{H}}$ represents two standard deviations in $\ln X_{\mathrm{H},0}$ from its expectation $\ln \overline{X}_{\mathrm{H},0}$, which is equivalent to variations in $X_{\mathrm{H},0}$ within the interval $X_{\mathrm{H},0}/\mathrm{UF}_{\mathrm{H}}$ and $X_{\mathrm{H},0}\mathrm{UF}_{\mathrm{H}}$. In this model, the variance of $\ln X_{\mathrm{H},0}$ is constant with temperature and can therefore be written as $\mathrm{var}[\ln X_{\mathrm{H},0}] = \sigma_{\mathrm{H}}^2$. The variance of $X_{\mathrm{H},0}$ is $\mathrm{var}[X_{\mathrm{H},0}] = \overline{X}_{\mathrm{H},0}^2[\exp(2\sigma_{\mathrm{H}}^2) - \exp(\sigma_{\mathrm{H}}^2)]$, which increases with temperature in the same manner as $\overline{X}_{\mathrm{H},0}^2$. Using a variance estimator for the data in Figure 2 and Eq. (3.2), the uncertainty factor of the H-impurities concentration is estimated to be $\mathrm{UF}_{\mathrm{H}} \simeq 41$, which gives an expectation $\mathrm{E}[X_{\mathrm{H},0}] = 5.61\overline{X}_{\mathrm{H},0}$.

Notice that, in general, the total amount of uncertainty in the distribution of impurities may be different from the uncertainty solely quantified by the data scatter, since each of the individual points in Figure 2 is subject to experimental errors. However, in case of they are important, these experimental errors would only increase the uncertainty factor UF_{H}. Additionally, different values of A, $T_{a,\mathrm{H}}$ and UF_{H} may be obtained depending on the data subset chosen in Figure 2. The present model for the PDF $P(X_{\mathrm{H},0})$ of the

impurities concentration may be considered as a first approximation in an escalation of difficulty. Further research may be required to propose more rigorous models.

Regarding the activation process depicted in Figure 2 and described in Eq. (3.1), it may be tempting to explain the production of H impurities by arguing that they have been generated by $C-H$ bond breaking. Note that the $C-H$ bond dissociation energy remains roughly of the same order of magnitude across a wide span of hydrocarbons, with a typical activation temperature of $\sim 50{\cdot}10^3$ K. However, the H−impurities concentration $X_{H,0}$ in Figure 2 has an activation temperature $T_{a,H} = 12916$ K when data points from both $\mathcal{M}_1$ and $\mathcal{M}_2$ methods are retained for the least-squares, $T_{a,H} = 7570$ K for data points of method $\mathcal{M}_1$ only, and $T_{a,H} = 14131$ K for data points of method $\mathcal{M}_2$ only. The discrepancies in the experimental activation temperatures with respect to the mean $C-H$ bond activation temperature indicate that there may be more complex chemical processes at play and, as emphasized above, that the theory for the presence of H impurities in shock tubes outlined here is only qualitative.

4. Effects of residual impurities on ignition above crossover

In this section, insight is gained about the physics of the interaction between radical impurities and the main test gases during the ignition process above crossover. The theoretical analysis follows and briefly extends the seminal work of Del Álamo *et al.* (2010) in order to account for residual impurities in hydrogen ignition employing a 5-step short chemistry. In addition, computations are performed using Flamemaster and the Stanford chemical mechanism for detailed H_2/O_2 kinetic descriptions.

The crossover temperature T_c in H_2/O_2 combustion, which increases with increasing pressure ($T_c \sim 950$ K at $p = 1$ bar), is typically defined as the limit temperature in which the main branching $H + O_2 \rightarrow OH + O$ and termination $H + O_2 + M \rightarrow HO_2 + M$ reaction rates become equal up to the multiplicative branching factor, $k_{2f}[M] = 2k_{1f}$, with $[M] = p/R^0T$ the molar concentration of the diluent gas and R^0 the universal gas constant. Below the atmospheric pressure, the crossover temperature indicates the second-explosion limit, in which rapid chain-branching reactions lead to the build up of active radicals that are subsequently depleted in slow exothermic recombination steps. Near the atmospheric pressure and above, the crossover temperature represents the boundary between the strong-ignition region at $T > T_c$, in which the description of the branched-chain explosions in the second limit holds to a good extent, and the weak-ignition region $T < T_c$ (yet above the third limit), in which a much slower branching path involving HO_2 and H_2O_2 leads to thermal explosion (see Figure 1).

4.1. *Theory of* H_2/O_2 *ignition assisted by* H *impurities*

Following Del Álamo *et al.* (2010), for $T > T_c$ the rapid chain-branching dynamics starts with the production of H and OH radicals from collisions between H_2 and O_2 molecules through the main initiation reaction

$$\text{(13b)} \qquad H_2 + O_2 \rightarrow HO_2 + H,$$

with $k_{13b} = 0.75 \cdot 10^6 T^{2.43} \exp(-26926\text{K}/T)(\text{cm}^3\text{mol}^{-1}\text{s}^{-1})$. The reaction numbering follows the reference-mechanism notation of Hong *et al.* (2011). The alternate chain-initiation step $H_2 + O_2 \rightarrow OH + OH$ is not included in the reference mechanism in accord with ab-initio computations that relegate it to highly unlikely events (Hong *et al.* 2011). A characteristic initiation time t_I associated with (13b) can be defined as $t_I =$

$(k_{13b}[O_2]_0)^{-1}$, with the subindex $_0$ indicating initial values. In particular, t_I represents the timescale over which H atoms are formed in amounts of order $[H_2]_0$.

When the concentration of H radicals generated by (13b) is sufficiently large, a branched-chain process follows, which can be described by the steps

$$\begin{aligned} &\text{(1f)} \quad H + O_2 \rightarrow OH + O \\ &\text{(9f)} \quad H_2 + O \rightarrow H + OH \\ &\text{(10f)} \quad H_2 + OH \rightarrow H_2O + H, \end{aligned}$$

where (1f) and (9f) are chain-branching reactions and (10f) is a chain-propagation step. Inspection of these chemical steps shows that two H atoms are formed by (9f) and (10f) for each H atom consumed in (1f), which leads to a rapid build up of H radicals. Similar considerations can be used to describe the multiplication of OH radicals. The corresponding rates of these steps are $k_{1f} = 1.04 \cdot 10^{14} \exp(-7701\text{K}/T)$ ($\text{cm}^3\text{mol}^{-1}\text{s}^{-1}$), $k_{9f} = 3.82 \cdot 10^{12} \exp(-4000\text{K}/T) + 8.79 \cdot 10^{14} \exp(-9650\text{K}/T)$ ($\text{cm}^3\text{mol}^{-1}\text{s}^{-1}$), and $k_{10f} = 2.17 \cdot 10^{8} \exp(-1740\text{K}/T)$ ($\text{cm}^3\text{mol}^{-1}\text{s}^{-1}$).

Upon induction, the radicals are depleted in direct recombination reactions (2f, 7b, 18b, 19f, 20f), which are responsible for the heat release and the corresponding temperature increment. Out of these steps, the fastest termination reaction is found to be

$$\text{(2f)} \quad H + O_2 + M \rightarrow HO_2 + M,$$

where M denotes the collider. The termination step (2f) is subject to the fall-off effect, which is neglected in this study (a good approximation for not too high pressures). The rate of (2f) is $k_{2f} = 6.81 \cdot 10^{18} T^{-1.2}$ ($\text{cm}^6\text{mol}^{-2}\text{s}^{-1}$). Following (2f), the HO_2 radical forms stable species before doing anything else and the chain is terminated. A characteristic termination time t_T associated with (2f) can be defined as $t_T = (k_{2f}[M][O_2]_0)^{-1}$.

The set (13b)-(1f)-(9f)-(10f)-(2f) represents the 5-step short mechanism of Del Álamo *et al.* (2010), the accuracy of which was tested thoroughly in earlier work (see for instance Figure 3 in Del Álamo *et al.* (2010)). Briefly, the 5-step mechanism is accurate in an intermediate range of temperatures, but it fails at high temperatures ($\gtrsim 2500$ K) because of the absence of dissociation reactions in the description, and at low temperatures and high pressures (near and below crossover) because it does not account for HO_2 and H_2O_2 chemistry.

When the short mechanism (13b)-(1f)-(9f)-(10f)-(2f) is used, and since the reactant consumption and the temperature increment are negligible during the induction period, the species conservation equations for the radicals become

$$\frac{dy_H}{d\tau} = -\left(\gamma + \frac{1}{2}\right) y_H + \frac{y_O}{2} + \frac{y_{OH}}{2} + \epsilon, \tag{4.1}$$

$$\frac{dy_O}{d\tau} = \frac{\phi}{\kappa_O} \left(y_H - y_O\right), \tag{4.2}$$

$$\frac{dy_{OH}}{d\tau} = \frac{\phi}{\kappa_{OH}} \left(y_H + y_O - y_{OH}\right), \tag{4.3}$$

where $y_H = [H]/[H_2]_0$, $y_O = [O]/(\kappa_O[O_2]_0)$ and $y_{OH} = [OH]/(\kappa_{OH}[O_2]_0)$ are the dimensionless radical concentrations, and $\tau = t/(2k_{1f}[O_2]_0)$ is the nondimensional time. Similarly, $\kappa_{OH} = k_{1f}/k_{10f}$ and $\kappa_O = k_{1f}/k_{9f}$ are dimensionless ratios of OH and O consumption rates, respectively, and $\phi = [H_2]_0/2[O_2]_0$ is the equivalence ratio of the gaseous mixture. Note that $\kappa_O[O_2]_0$ and $\kappa_{OH}[O_2]_0$ are the characteristic steady-state

concentrations of O and OH radicals, respectively. Additionally,

$$\epsilon = \frac{t_B}{t_I} = \frac{k_{13b}}{2k_{1f}} \tag{4.4}$$

is the ratio of the branching-to-initiation characteristic times, and

$$\gamma = \frac{t_B}{t_T} = \frac{k_{2f}[\mathrm{M}]}{2k_{1f}} \tag{4.5}$$

is the ratio of the branching-to-termination characteristic times, which increases with increasing pressure and decreasing temperature. The value $\gamma = 1$ indicates the second explosion limit. For $\gamma > 1$, the branching dynamics is much slower than the termination, and the ignition process is extremely slow. For $\gamma < 1$, the branching timescale is smaller than the characteristic termination time, which rapidly leads to ignition. In the ignition zone, for $\gamma < \epsilon \ll 1$ (which occurs at high temperatures) the ordering of time scales is $t_B \ll t_I < t_T$. Conversely, for $\epsilon \ll \gamma < 1$ (which occurs at moderate-to-low temperatures), the ordering of time scales becomes $t_B < t_T \ll t_I$.

Equations (4.1)-(4.3) are subject to the initial conditions

$$y_{\mathrm{H}} = \xi_{\mathrm{H}}, \quad y_{\mathrm{OH}} = \xi_{\mathrm{OH}} \quad \text{and} \quad y_{\mathrm{O}} = \xi_{\mathrm{O}} \tag{4.6}$$

at $\tau = 0$, where $\xi_{\mathrm{H}} = X_{\mathrm{H},0}/X_{\mathrm{H}_2}$. In this formulation, $X_{\mathrm{H},0}$ is given by sampling the distribution (3.1)-(3.2).

To calculate the autoignition time, a threshold value for the radical concentrations computed from (4.1)-(4.3) and (4.6) needs to be specified. Here, ignition is associated with the instant in which reaction $\mathrm{H} + \mathrm{O}_2 \leftrightharpoons \mathrm{OH} + \mathrm{O}$ reaches partial equilibrium, or equivalently, when the relation $2\phi K_1/(\kappa_{\mathrm{O}}\kappa_{\mathrm{OH}}) = y_{\mathrm{O}}y_{\mathrm{OH}}/y_{\mathrm{H}}$ is satisfied. In this formulation, K_1 is the equilibrium constant of step $\mathrm{H}+\mathrm{O}_2 \leftrightharpoons \mathrm{OH}+\mathrm{O}$. The resulting autoignition time is found not to depend much on this selection (Del Álamo *et al.* 2010).

The system (4.1)-(4.3) has two complex conjugate eigenvalues with negative real parts and a real eigenvalue λ_1, which becomes positive for $\gamma < 1$ and negative for $\gamma > 1$. The solution for the autoignition time, which accounts for $\xi_{\mathrm{H}} > 0$, $\xi_{\mathrm{O}} > 0$ and $\xi_{\mathrm{OH}} > 0$ in (4.6), is given by

$$t_{ig} = \frac{1}{2k_{1f}[\mathrm{O}_2]_0\lambda_1} \ln\left(\frac{2C_{11}\phi K_1}{b_1 C_{12} C_{13} \kappa_{\mathrm{O}}\kappa_{\mathrm{OH}}}\right), \tag{4.7}$$

where C_{1i} are the components of the λ_1-eigenvector $\mathbf{C_1}$ of the coefficient matrix in the linear system (4.1)-(4.3). Additionally, b_1 is a constant that depends on the initial conditions (4.6) and is calculated by imposing that $\mathbf{q}(\tau = 0) = \mathbf{C}^{-1}(\boldsymbol{\xi} - \mathbf{y_p})$, where $\mathbf{q} = [b_1 \mathrm{e}^{\lambda_1\tau}, b_2\mathrm{e}^{\lambda_2\tau}, b_3\mathrm{e}^{\lambda_3\tau}]^{\mathrm{T}}$, $\mathbf{C}$ is the matrix of eigenvectors, $\boldsymbol{\xi} = [\xi_{\mathrm{H}}, \xi_{\mathrm{O}}, \xi_{\mathrm{OH}}]^{\mathrm{T}}$ is the vector of initial conditions, and $\mathbf{y}_p = [-\epsilon/(1-\gamma), -\epsilon/(1-\gamma), -2\epsilon/(1-\gamma)]$ is the particular solution of (4.1)-(4.3).

Equation (4.7) is essentially the same formula as the one obtained by Del Álamo *et al.* (2010) with the only difference that the constant b_1 retains here the initial conditions for the radical concentrations, which were set to zero in Del Álamo *et al.* (2010) and which play a central role here.

For rich to stoichiometric mixtures, $\phi \gtrsim 1$, eqs. (4.1) and (4.2) suggest that variations in y_{O} and y_{OH} occur in a much faster time scale than the variations of y_{H}. In particular, after short dimensionless times of order $\tau \sim 1/\phi$, the information of the initial concentrations ξ_{O} and ξ_{OH} is lost and the O and OH atoms reach steady state with $y_{\mathrm{H}} \sim y_{\mathrm{O}}$ and $y_{\mathrm{OH}} \sim 2y_{\mathrm{H}}$. In this limit, Eq. (4.1) can be integrated to give the time evolution of the

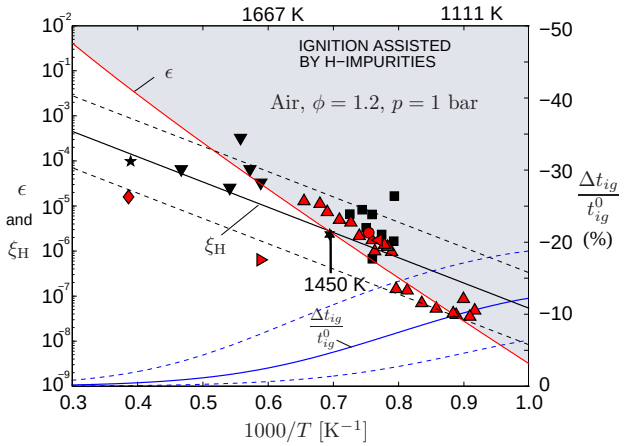

FIGURE 3. Effects of uncertainties in the residual impurities on the autoignition time variations (4.11) calculated from the solution to the reduced-order ignition problem (4.1)-(4.3) subject to (4.6). Solid and dashed lines indicate mean and mean ± standard deviation respectively. The symbols denote the same experimental data points shown in Figure 2.

concentration $y_{\rm H}$. For $t_{ig}/t_B \gg 1 \gtrsim 1/\phi$, the ignition time

$$t_{ig,R} \simeq \frac{1}{2k_{1f}[{\rm O}_2]_0(1-\gamma)} \ln\left\{\frac{\phi K_1}{\kappa_{\rm O}\kappa_{\rm OH}[\xi_{\rm H}+\epsilon/(1-\gamma)]}\right\} \tag{4.8}$$

is obtained. The validity of Eq. (4.8) extends from rich mixtures $\phi \gg 1$ to near stoichiometric mixtures $\phi \sim 1$. In view of Eq. (4.8), a competition occurs between the kinetic parameter $\epsilon/(1-\gamma)$ and the dimensionless concentration of impurities $\xi_{\rm H}$. The H−impurities become important if

$$\xi_{\rm H} \gtrsim \epsilon/(1-\gamma), \tag{4.9}$$

or equivalently, if

$$X_{{\rm H},0}/t_B \gtrsim k_{13b}X_{{\rm H}_2,0}X_{{\rm O}_2,0}p/({\rm R}^0T), \tag{4.10}$$

which corresponds to the limit in which the molar fraction of the H−impurities is larger than the molar fraction of H generated by the initiation step (13b) during a characteristic branching time t_B.

The relative variation in the autoignition time produced by H−impurities is defined as

$$\Delta t_{ig}/t^0_{ig} = (t_{ig} - t^0_{ig})/t^0_{ig}. \tag{4.11}$$

Here, t^0_{ig} is the nominal autoignition time calculated with the tabulated rate constants of the corresponding mechanism and zero initial H−impurities, $X_{{\rm H},0} = 0$, where the symbol X denotes the molar fraction. In particular, Eq. (4.8) shows that the autoignition time is bounded by the upper limit $t^0_{ig,R}$, in that $t_{ig,R}$ is always smaller than $t^0_{ig,R}$ if impurities are present, with $t_{ig,R}$ tending to $t^0_{ig,R}$ from the left as $\xi_{\rm H} \to 0$.

Based on the criterion (4.9), Figure 3 shows the temperature dependence of the dimensionless parameters ϵ and $\xi_{\rm H}$ as well as the autoignition-time decrement caused by H−impurities, for both diluted and non-diluted conditions. In particular, it is observed that dilution increases the effects of the H−impurities, in that the effective value of $\xi_{\rm H}$ in (4.9) increases with increasing dilution because of the decrease in $X_{{\rm H}_2}$. The effects of the H−impurities increase as the temperature decreases (still above crossover) because of the

disparity in the slopes of ϵ and $\xi_{\rm H}$, which makes the initiation step (13b) become slower at a faster rate than the decrease in the speed of the activation process that leads to the generation of H impurities from the radical precursors. The effects of the H-impurities are largely independent of the pressure for moderate to high temperatures, for which $\gamma \ll 1$, but at low temperatures $\gamma \simeq 1$ an increase in pressure causes a faster termination rate, which in turn reduces the effects of contamination of the shock tube on the delay time. Overall, autoignition-time decrements of order 15% for air and of order 30% for 99.2%-Ar diluted mixtures are predicted by this model in the low-temperature end, with increasing variance and increasing departures from the nominal autoignition time t^0_{ig} as the temperature decreases. These asymptotic estimates are consistent with the findings shown below, where the full mechanism is used for calculations.

In the limit in which the amount of impurities is -with high probabilities- very small compared to the amount of H atoms generated by the initiation step (13b) during a characteristic branching time, $P[\xi_{\rm H} \ll \epsilon/(1-\gamma)] \to 1$, which typically occurs at high temperatures, a series expansion of (4.8) gives

$$t_{ig,R} = t^0_{ig,R} - \frac{1}{2k_{1f}[{\rm O}_2]_0(1-\gamma)}\left\{\left(\frac{(1-\gamma)\xi_{\rm H}}{\epsilon}\right) + O\left[\left(\frac{(1-\gamma)\xi_{\rm H}}{\epsilon}\right)^2\right]\right\}. \tag{4.12}$$

Equation (4.12) shows that, in this limit, the ignition-time decrement is log-normally distributed to second order in $(1-\gamma)\xi_{\rm H}/\epsilon$ if the model for H$-$impurities (3.1)-(3.2) is used, with expectation and variance given by

$$\mathrm{E}[t_{ig,R}] \simeq t^0_{ig,R} - \frac{1}{2k_{1f}[{\rm O}_2]_0}\left(\frac{\mathrm{E}[\xi_{\rm H}]}{\epsilon}\right) \tag{4.13}$$

and

$$\mathrm{var}[t_{ig,R}] \simeq \frac{1}{4k^2_{1f}[{\rm O}_2]^2_0}\left(\frac{\mathrm{var}[\xi_{\rm H}]}{\epsilon^2}\right), \tag{4.14}$$

where $\mathrm{E}[\xi_{\rm H}] = \mathrm{e}^{\sigma^2_{\rm H}/2}\overline{\xi}_{\rm H}$, $\mathrm{var}[\xi_{\rm H}] = (\mathrm{e}^{2\sigma^2_{\rm H}} - \mathrm{e}^{\sigma^2_{\rm H}})\overline{\xi}^2_{\rm H}$, $\overline{\xi}_{\rm H} = \overline{X}_{{\rm H},0}/X_{{\rm H}_2,0}$ and $\sigma_{\rm H}$ is given in (3.2). Equations (4.13) and (4.14) state the linearity between the mean and variance of the autoignition time and the impurities, and in particular, they reveal that both the mean deviation from the nominal autoignition time $t^0_{ig,R} - \mathrm{E}[t_{ig,R}]$ and its variance $\mathrm{var}[t_{ig,R}]$ increase with decreasing temperature, as shown in Figure 3.

In the opposite limit, namely the limit in which the amount of impurities is -with high probabilities- very large compared to the amount of H atoms generated by the initiation step (13b) during a characteristic branching time, $P[\xi_{\rm H} \gg \epsilon/(1-\gamma)] \to 1$, which typically occurs at low temperatures (still above crossover), the ignition delay asymptotes to

$$t_{ig,R} = \frac{1}{2k_{1f}[{\rm O}_2]_0(1-\gamma)}\left\{\ln\left(\frac{\phi K_1}{\kappa_{\rm O}\kappa_{\rm OH}\xi_{\rm H}}\right) - \left(\frac{\epsilon}{\xi_{\rm H}}\right) + O\left[\left(\frac{\epsilon}{\xi_{\rm H}}\right)^2\right]\right\}. \tag{4.15}$$

The leading-order approximation in (4.15) predicts a Gaussian distribution for $t_{ig,R}$ if the model for H$-$impurities (3.1)-(3.2) is used, which contradicts the physical constraint that $t_{ig,R} < t^0_{ig,R}$. To compensate for this, the second approximation in (4.15), which has a lognormal distribution and sweeps out the high-$t_{ig,R}$ tail of the leading-order Gaussian distribution. The resulting distribution of $t_{ig,R}$ has a distribution with expectation and

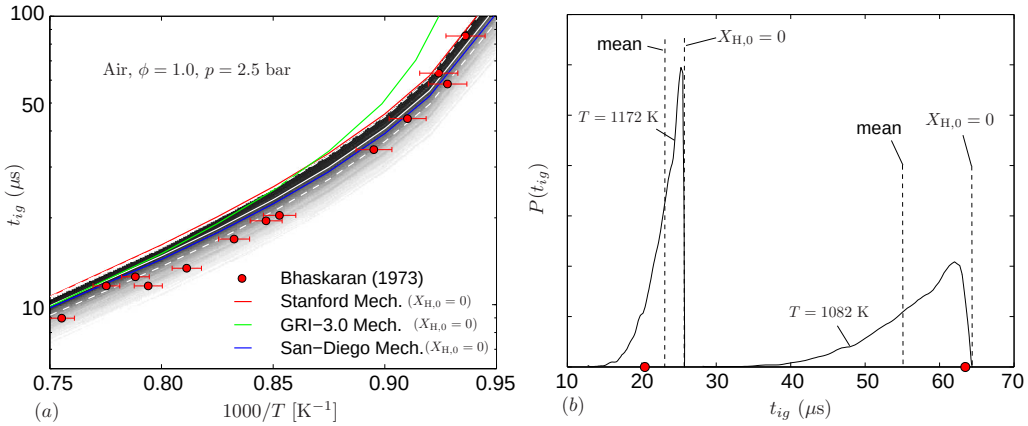

FIGURE 4. (a) Contours of the PDF of the ignition time $P(t_{ig})$ for H_2/air mixtures after $2 \cdot 10^5$ samples of the concentration of H−impurities, calculated using the Stanford mechanism Hong *et al.* (2011), together with Bhaskaran et al.'s experiments (Bhaskaran *et al.* 1973) (red dots), with darker regions indicating high probability. Panel (a) shows 1% error bars in temperature around experimental points, the mean $\mathrm{E}[t_{ig}]$ (solid white line), $\mathrm{E}[t_{ig}] \pm$ standard deviation (dashed white line), and deterministic calculations of t_{ig} calculated with $X_{\mathrm{H},0} = 0$ using the Stanford mechanism (red solid line) (Hong *et al.* 2011), the San Diego mechanism (blue solid line) (Saxena *et al.* 2006) and the GRI v3.0 mechanism (green solid line) (Smith *et al.* 2011). Panel (b) shows scaled PDFs $P(t_{ig})$ at two different temperatures for the same pressure and mixture composition as in (a), with dots (red color online) indicating experimental data at the corresponding temperature.

variance given by

$$\mathrm{E}[t_{ig,R}] \simeq t^0_{ig,R} - \frac{1}{2k_{1f}[\mathrm{O}_2]_0(1-\gamma)} \left\{ \ln\left[\frac{(1-\gamma)}{\epsilon}\right] + \mathrm{E}[\ln \xi_{\mathrm{H}}] + \epsilon \mathrm{E}\left[\frac{1}{\xi_{\mathrm{H}}}\right] \right\}, \qquad (4.16)$$

and

$$\mathrm{var}[t_{ig,R}] \simeq \frac{1}{4k^2_{1f}[\mathrm{O}_2]^2_0(1-\gamma)^2} \left\{ \mathrm{var}[\ln \xi_{\mathrm{H}}] + \epsilon^2 \mathrm{var}\left[\frac{1}{\xi_{\mathrm{H}}}\right] \right\}, \qquad (4.17)$$

where $\mathrm{E}[\ln \xi_{\mathrm{H}}] = \ln \overline{\xi}_{\mathrm{H}}$, $\mathrm{E}[1/\xi_{\mathrm{H}}] = \mathrm{e}^{\sigma^2_{\mathrm{H}}/2}/\overline{\xi}_{\mathrm{H}}$, $\mathrm{var}[\ln \xi_{\mathrm{H}}] = \sigma^2_{\mathrm{H}}$, $\mathrm{var}[1/\xi_{\mathrm{H}}] = (\mathrm{e}^{2\sigma^2_{\mathrm{H}}} - \mathrm{e}^{\sigma^2_{\mathrm{H}}})/\overline{\xi}^2_{\mathrm{H}}$, $\overline{\xi}_{\mathrm{H}} = \overline{X}_{\mathrm{H},0}/X_{\mathrm{H}_2,0}$ and σ_{H} is given in (3.2). Equations (4.16) indicate an intricate temperature dependence of the variance $\mathrm{var}[t_{ig,R}]$ and mean deviation $t^0_{ig,R} - \mathrm{E}[t_{ig,R}]$.

It is therefore observed that the PDFs of the ignition time transit from lognormal to near-normal as the temperature decreases.

4.2. *Detailed-chemistry computations of ignition assisted by* H−*impurities*

Numerical simulations with Flamemaster are performed to integrate the accumulation-reaction conservation equations with detailed H_2/O_2 chemistry under uncertainties in H−impurities, and comparisons are made with experimental data. The calculations are carried out for conditions above and below crossover. The detailed kinetics used in the computations is the Stanford H_2/O_2 chemical mechanism of (Hong *et al.* 2011), but also the San Diego (Saxena *et al.* 2006) and GRI v3.0 (Smith *et al.* 2011) kinetic descriptions are used for comparisons.

In all the computations shown below, a characteristic error in the test temperature $\Delta T = 10$ K has been included, the reason being that in shock tubes the post-shock temperature is estimated by substituting in the Rankine-Hugoniot equations the shock

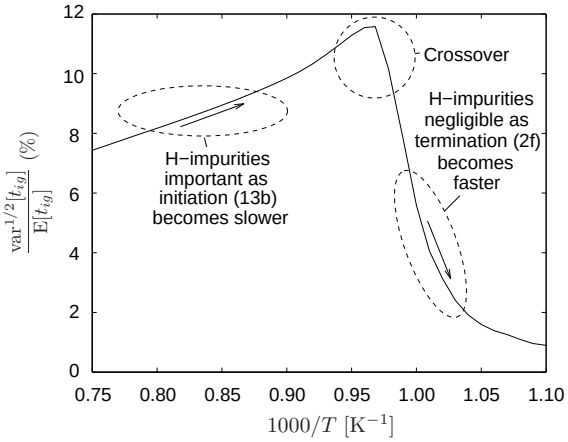

FIGURE 5. Dimensionless standard deviation induced by the uncertainties in H−impurities on the ignition time calculated using the Stanford mechanism Hong *et al.* (2011) after $2{\cdot}10^5$ samples, for H_2/air, $\phi = 1.0$ and $p = 2.5$ bar. The mean deviation $\mathrm{E}[t_{ig}] - t_{ig}^0$ follows a similar trend with decreasing temperature as the standard deviation shown here.

speed, which is obtained by a procedure that involves the detection of the shock by pressure transducers and the differentiation of its position in time, giving errors of order 10 K in the temperature. Further details are given in Herbon (2004). As shown below, this uncertainty in the temperature produces non-negligible uncertainties in the ignition time, which are comparable to the uncertainties induced by impurities and to the variabilities obtained by using two other chemical mechanisms. However, a rigorous treatment of the effects of temperature uncertainties is not pursued in this work, and requires further investigations.

Figure 4 shows comparisons of the computations of ignition under uncertainties in the H−impurities with experimental data of Bhaskaran *et al.* (1973). In these calculations, the uncertainty model (3.1)-(3.2) has been used for the H−impurities. It is worth noticing that for the air case in Figure 4, the effect of the temperature uncertainty, the variabilities among different mechanisms and the uncertainties induced by the impurities are all within the same range with regard to their effects on the ignition time. Computations not shown here demonstrate that in the case of highly diluted mixtures, the uncertainties in t_{ig} induced by the impurities tend to dominate everything else (Urzay *et al.* 2014).

In these calculations, the global trends shown by the theoretical analyses in the previous subsection are confirmed, in that the PDF transits from lognormal to a 'nearly-Gaussian' distribution as temperature decreases (still above crossover), as predicted by the theory.

Additionally, Figure 5 shows that the variance $\mathrm{var}[t_{ig}]$ and mean deviation $\mathrm{E}[t_{ig}] - t_{ig}^0$ increase as the temperature decreases until crossover is reached. Below crossover, both magnitudes decay rapidly with decreasing temperatures. The effects of H impurities below crossover are negligible. Note that the theoretical model in Section 4 and the original impurity-less formulation of Del Álamo *et al.* (2010) does not include the chemistry near crossover, and therefore this effect could not be captured. The reasoning behind the vanishing effect of H-impurities below crossover is explained in what follows.

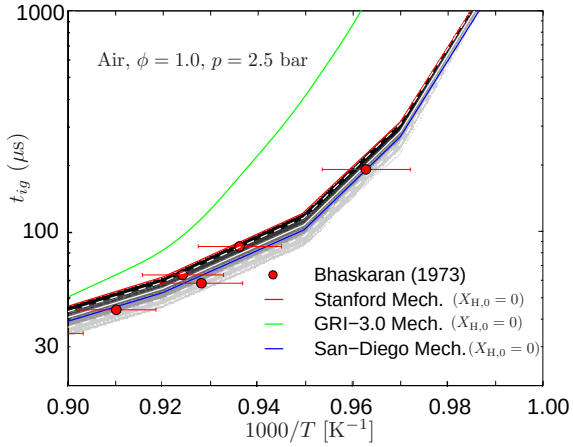

FIGURE 6. Effects of uncertainties in the residual impurities on the autoignition time near crossover. The figure shows PDFs $P(t_{ig})$ after $2 \cdot 10^5$ simulations, for ignition in air/H_2 mixtures calculated using the Stanford mechanism (Hong *et al.* 2011), together with Bhaskaran et al. (Bhaskaran *et al.* 1973) experiments (red dots). Also shown are 1% error bars in temperature around experimental points, E$[t_{ig}]$ (solid white line), E$[t_{ig}]$ $\pm$ standard deviation (dashed white line), and deterministic calculations of t_{ig} calculated with $X_{H,0} = 0$ using the Stanford mechanism (red solid line) (Hong *et al.* 2011), the San Diego mechanism (blue solid line) (Saxena *et al.* 2006), and the GRI v3.0 mechanism (green solid line) (Smith *et al.* 2011).

5. Effects of residual impurities on ignition near and below crossover

At temperatures below crossover, the parameter γ in (4.5) is $\gamma > 1$, indicating that the branching step (1f) is slower than the termination reaction (2f). Therefore, all radicals tend to be removed rapidly by (2f) with a time constant that decreases with decreasing temperature and increasing pressure. Below crossover, $\gamma > 1$, the ordering of time scales becomes $t_T < t_B \ll t_I$. In the description made by Treviño (1991) of ignition below crossover, the step (2f) generates HO_2 upon removing H radicals. The resulting HO_2 forms H_2O_2 through the steps (6f) $HO_2 + HO_2 \rightarrow H_2O_2 + O_2$ and (15b) $HO_2 + H_2 \rightarrow H_2O_2$+H. The H_2O_2 is subsequently depleted in the exothermic reaction (3f) H_2O_2+M $\rightarrow$ OH + OH + M.

The slowest step among (13b)-(1f)-(9f)-(10f)-(2f)-(6f)-(15b)-(3f) at low temperatures tends to be (3f), which sets the ignition time in the first approximation, with HO_2 being approximately in steady state (Boivin *et al.* 2012). Because of the rapid removal of radicals by the fast termination step (2f), the H−impurities play a very modest role in ignition below crossover, as confirmed in the calculations shown in Figure 6.

The long test times make measurements of ignition times below crossover in shock tubes particularly difficult for a number of reasons, among which the most important ones seem to be the hydrodynamic and non-ideal pressure-rise in the shock tube during the experimental time window (Davidson & Hanson 2004; Ihme *et al.* 2013). An interesting question is whether the impurities in shock tubes may have comparable effects to the shift in the ignition time caused by non-ideal pressure rise. Although the computations in Figure 6 show some effect of impurities in the near-crossover region in the H_2−air experiments of Bhaskaran *et al.* (1973), these experiments did not fully reach below-crossover temperatures. On the other hand, computations not shown here conclude that the effects of H−impurities below crossover in highly diluted mixtures are practically negligible compared to non-ideal or hydrodynamic effects (Urzay *et al.* 2014).

6. Conclusions

In this study the influences of impurities on the calculation and experimental determination of ignition times in H_2/O_2 mixtures were addressed, with particular emphasis on the uncontrolled presence of residual H-atoms in shock tubes. Two methods were proposed for quantifying experimentally the H-residual impurities in shock tubes. Based on experimental data, a stochastic Arrhenius model for the H−impurities was proposed. Using this model, theoretical quantifications of the uncertainties induced by the impurities on autoignition times were performed by using a short 5-step chemistry, which showed that the relative effects of H-impurities delay times above crossover become increasingly large as the dilution increases and as the temperature and pressure decrease, reaching their maximum importance near crossover. Below crossover, the effects of the impurities on ignition delay decay rapidly and are negligible compared to the departures produced by the non-ideal pressure-rise effects typically found in shock-tube experiments at such long test times.

For the conditions tested, and according to the short mechanism used here, computations not shown here reveal that the effects of chemical-kinetic uncertainties on the ignition time, including the effects of correlations between uncertainties in branching and termination rates, were typically negligible compared to the effects of the uncertainties induced by the H-impurities in the shock tube (Urzay *et al.* 2014). Exceptions to this conclusion occur at high temperatures in air, for which the effects of the impurities are less important and chemical-kinetic uncertainties dominate in the quantification of uncertainties in the ignition time.

In conclusion, the results obtained in this study suggest that a quantification of residual impurities in the shock tube may be needed prior to undertaking any tuning of the kinetic parameters to match H_2/O_2 ignition targets. Further details on methodologies for quantifying the level of impurities in shock tubes can be found in Urzay *et al.* (2014).

7. Acknowledgments

This investigation was funded by the Predictive-Science Academic-Alliance Program (PSAAP), DoE Grant # DE-FC52-08NA28614. JU was supported by the 2011-2012 Postdoctoral Fellowship for Excellence in Research, Ibercaja Foundation (Zaragoza, Spain).

REFERENCES

Bhaskaran, K. A., Guptan, M. C. & Just, T. 1973 Shock-tube study of the effect of unsymmetric dimethyl hydrazine on the ignition characteristics of hydrogen-air mixtures. *Comb Flame.*, 21:45-48.

Boivin, P., Sánchez, A. L. & Williams, F. A. 2012 Explicit analytic prediction for hydrogenoxygen ignition times at temperatures below crossover. *Comb. Flame*, 159: 748-752.

Davidson, D. F. & Hanson, R. K. 2004 Interpreting shock-tube data. *Int. J. Chem. Kin.*, 36:510-523.

Davidson, D. F., Petersen, E. L., Röhrig, M., Hanson, R. K. & Bowman, C. T. 1996 Measurement of the rate coefficient of $H + O_2 + M \rightarrow HO_2 + M$ for M = Ar and N_2 at high pressures. *Proc. Comb. Inst.*, 26:481-488.

Del Álamo, G., Williams, F. A. & Sánchez, A. L. 2010 Hydrogen-oxygen induction times above crossover temperatures. *Comb. Sci. and Tech.*, 176:1599-1626.

Herbon, J. T., Hanson, R. K., Golden, D. M. & Bowman, C. T. 2002 A shock tube study of the enthalpy of formation of OH. *Proc. Comb. Inst.*, 29:1201-1208.

Herbon, J. T. 2004 *Shock tube measurements of* $CH_3 + O_2$ *kinetics and the heat of formation of the* OH *radical*, Ph.D. Thesis, Stanford University.

Hong, Z., Davidson, D. F. & Hanson R. K. 2011 An improved H_2/O_2 mechanism based on recent shock tube / laser absorption measurements. *Comb. Flame*, 158(1): 633–644.

Ihme, M., Sung, Y. & Deiterding, R. 2013 Detailed Simulations of shock-bifurcation and ignition of an argon-diluted hydrogen/oxygen mixture in a shock tube. *AIAA Paper* 2013-0538:1-14.

Li, H. 2007 *Near-infrared diode laser absorption spectroscopy with applications to reactive systems and combustion control*, Ph.D. Thesis, Stanford University.

Lewis, B. & von Elbe, G. 1961 *Combustion, flames, and explosions of gases*, 2nd Ed., Academic Press.

Petersen, E. L. 1998 *A shock tube and diagnostics for chemistry measurements at elevated pressures with application to methane ignition*, Ph.D. Thesis, Stanford University.

Masten, D. A., Hanson, R. K. & Bowman, C. T. 1990 Shock tube study of the reaction $H+O_2 \rightarrow O+OH$ using OH laser absorption. *J. Phys. Chem.*, 94:7119-7128.

Nuclear and Industrial Safety Agency of Japan. An explosion caused by hydrogen at Unit 3 of Fukushima Dai-ichi nuclear power plant. *NISA Press Release*, March 14, 2011.

Sánchez, A. L., Fernández-Tarrazo, E. & Williams, F. A. 2014 The chemistry involved in the third explosion limit of H_2-O_2 mixtures. *Combust. Flame*, 161:111-117.

Saxena, P. & Williams, F. A. 2006 Testing a small detailed chemical-kinetic mechanism for the combustion of hydrogen and carbon monoxide. *Comb. Flame*, 145: 316-323.

Smith, G. P.,Golden, D. M., Frenklach, M., Moriarty, N. W., Eiteneer, B., Goldenberg, M., Bowman, C. T., Hanson, R. K., Song, S., Gardiner, W. C., Lissianski, V. V. & Qin, Z. 2011GRI v3.0 mechanism. *http://www.me.berkeley.edu/gri_mech/*

Treviño, C. 1991 Ignition phenomena in H_2/O_2 mixtures. *Prog. Astronaut. Aeronaut.*, 131:19-43.

United States Nuclear Regulatory Commission. 1979 *Report of the President's Commission on the accident at Three-Mile Island.* Washington DC.

Urzay, J., Kseib, N., Davidson, D. F., Iaccarino, G. & Hanson, R. K. 2014 Uncertainty-quantification analysis of the effects of residual impurities on hydrogen-oxygen ignition in shock tubes. *Combust. Flame*, 161:1-14.

Vasu, S. S., Davidson, D. F. & Hanson, R. K. 2011 Shock tube study of syngas ignition in rich CO_2 mixtures and determination of the rate $H + O_2 + CO_2 \rightarrow HO_2 + CO_2$. *Energy Fuels*, 25:990-997.

Vasudevan, V. 2007 *Shock tube measurements of elementary oxidation and decomposition reactions important in combustion using* OH*,* CH*, and* NCN *laser absorption*, Ph.D. Thesis, Stanford University.